Nanoscale

PAPER

View Article Online
View Journal | View Issue

Cite this: *Nanoscale*, 2016, **8**, 14950

Scaled down glass transition temperature in confined polymer nanofibers†

Hongxia Wang,[a,b] Tongxin Chang,[a,c] Xiaohui Li,[a,c] Weidong Zhang,[a,c] Zhijun Hu*[a,b,c] and Alain M. Jonas*[d]

Received 2nd June 2016,
Accepted 19th July 2016

DOI: 10.1039/c6nr04459j

www.rsc.org/nanoscale

Arrays of polymer nanostructures have been widely used in many novel devices and nanofabrication methods. The glass transition temperature, which is a key parameter influencing the long-term stability of polymer nanostructures, has not yet been systematically studied and well understood. Here we study this technological and fundamental issue with polymers of different values of molar mass M confined in nanocylinders of a varying diameter D. The glass transition temperature T_g loses its dependence on the molar mass for $D \lesssim 100$ nm, a range in which the relative depression of T_g varies as $D^{-0.44}$. For higher cylinder diameters, T_g progressively recovers its dependence on the molar mass. This is quantitatively reproduced by a model based on an equilibrium interfacial excess of free volume, which needs to be created unless provided by the chain ends. Our findings suggest that the structural perturbations during nanofabrication may strongly affect the long-term stability of arrays of polymer nanostructures.

Introduction

Polymer nanostructures characterized by spatial confinement and low dimensions have been widely used for new types of (opto)electronic devices, batteries, catalyses, or as temporary templates for nanofabrication.[1–4] Typically, arrays of polymer nanostructures can be high-throughput fabricated by nanolithography approaches or can be directly shaped by nanoembossing or template filling.[5–8] Although the processing methods and device integration of polymer nanostructure arrays have rapidly developed in the past few decades, experimental study on the confinement induced changes of dynamical and thermodynamic properties still remains a challenging and controversial area.[9] The thermodynamic and dynamic behaviors and properties are, however, essential to widen the potential application of polymer nanostructures in nanotechnology and in further development of nanolithography.

For crystallizable polymers, much progress has been made in studying the effects of confinement on the crystallization behaviors and structures. It has been clearly revealed that the nuclei formation has changed from heterogeneous nucleation to homogeneous nucleation.[10] As a result, the crystallization temperature is reduced to a lower temperature compared to that of the bulk counterparts. In addition, lamellae ordering and orientation have been found due to graphoepitaxial growth and entropy losses.[11,12] Furthermore, the confinement induced ordering and preferential orientation of polymer molecular and/or supramolecular structures translates into improved physical properties such as stronger mechanical strength,[13] lower coercive field,[14] higher thermal conductivity,[15] and improved charge mobility.[16]

For nanostructures of amorphous polymers, they may kinetically freeze to a solid-like glassy state when cooled below the glass transition temperature T_g after nanofabrication, due to an abrupt loss of local molecular mobility. Below T_g, structural relaxation of polymer nanostructures can occur and strongly impact the performance and lifetime of polymer devices or temporary templates. The structural relaxation can be accelerated with increasing temperature close to T_g. Therefore, T_g is an important parameter for the long-term stability of polymer nanostructures. Experiments performed on T_g of arrays of polymer nanostructures fabricated by nanolithography or template filling, however, revealed that the glass transition behavior in confinement is very complex. Mundra and Torkelson *et al.* investigated the T_g of poly(methyl methacrylate) (PMMA) nanostripe arrays fabricated using electron beam lithography and revealed substantial T_g reductions (~15 K) between the

[a]*College of Physics, Optoelectronics and Energy & Collaborative Innovation Center of Suzhou Nano Science and Technology, Soochow University, Suzhou 215006, China*
[b]*College of Chemistry, Chemical Engineering and Materials, Soochow University, Suzhou 215123, China. E-mail: zhijun.hu@suda.edu.cn*
[c]*Center for Soft Condensed Matter Physics and Interdisciplinary Research & Key Lab of Modern Optical Technologies of Education Ministry of China, Soochow University, Suzhou 215006, China*
[d]*Bio & Soft Matter, Institute of Condensed Matter and Nanosciences, Université catholique de Louvain, Croix du Sud 1/L7.04.02, B1348 Louvain-la-Neuve, Belgium. E-mail: alain.jonas@uclouvain.be*

†Electronic supplementary information (ESI) available. See DOI: 10.1039/c6nr04459j

nanostructures and the thin films.[17] For PMMA or polystyrene (PS) nanostripe arrays fabricated by nanoimprint lithography, Ding and Soles *et al.* found that the structural relaxation can be accelerated although no apparent change of T_g was observed.[18,19] For polystyrene nanofibers confined in confined anodic aluminum oxide (AAO) nanopores, an enhancement of chain mobility but unchanged T_g was observed by Shin and Russell *et al.*[20] Duran *et al.* reported, however, that the T_g of nanofibers consisting of poly(γ-bezyl-L-glutamate) synthesized in AAO templates was reduced by as much as 50 K.[21] To complicate the issue further, two thermal T_gs were observed in slowly cooled PMMA and poly(*n*-butyl methacrylate) nanofibers confined in AAO templates by Xue *et al.*[22,23] By using dielectric and Raman spectroscopies, Blaszczyk-Lezak and Mijangos *et al.* revealed that two opposite effects may influence the glassy dynamics of PMMA nanofibers confined in AAO templates:[24] the attractive and hydrogen bonding interfacial interaction with the walls of AAO templates which slow down the chain motions; the confinement effect which speeds-up the dynamics of the PMMA chains.

Despite significant activity in this area, it still remains difficult to experimentally and theoretically make a unique and unambiguous connection between confinement and T_g, preventing from predicting the stability of polymer nanostructures. For polymer nanostructures fabricated by scanning beam lithography methods, the surface chemical compositions may be modified due to the crosslinking or decomposition reactions. In addition, the fabricated polymer nanostructures are confined in an asymmetric geometry composition of a substrate and air. Alternatively, for polymer nanostructures fabricated from template filling, the attractive interfacial interactions between polymer nanostructures and surrounding environments play an important role in determining and making the glassy dynamics very complicated. In order to eliminate the potential attractive interfacial interactions between polymer nanostructures fabricated by template filling and surrounding nanopore's inner surfaces, and to simulate the nanofabrication process of polymer nanostructures by nanoembossing in which the template is usually coated with a monolayer of perfluorosilane for facilitating template separation, here we strongly confine PMMA in narrow channels of AAO coated with a monolayer of perfluorooctyltrichlorosilane deposited from the gas phase, leading to non-attractive inner pore surfaces. The absence of free surfaces and chain adsorption at the polymer–wall interfaces in our bi-dimensionally confined systems provides an ideal opportunity to thoroughly study the effect of geometrical confinement. PMMA is selected here because it has been widely used as a photoresist in electron beam lithography and nanoimprint lithography. As seen, only one T_g is observed for PMMA nanofibers confined in AAO templates with non-attractive inner pores. The maximum T_g reduction is as large as 64 K in the smallest nanopores (45 nm in diameter) with respect to the bulk. Additionally, the T_g loses its dependence on the molar mass for nanopore's diameter D smaller than ~100 nm, a range in which the relative depression of T_g varies as $D^{-0.44}$; this strong, observed decrease of T_g can be simply interpreted as arising from the accumulation of interfacial excess free volume which can be partially supplied by chain ends, without introducing new parameters.

Experimental

Materials and methods

Nanoporous AAO templates were prepared by a two-step anodization method. Typically, ultrapure aluminum foils (99.999%, 2 × 2 cm) were cleaned with an organic solvent, annealed at 723 K and electropolished in a solution of perchloric acid/ethanol (1/4 v/v) with an applied voltage of 30 V. After chemical etching with 0.3 M oxalic acid solution and voltage of 40 V, the first anodic layer was removed with a solution of mixed chromic acid and phosphoric acid. The second anodization was performed under similar conditions as the first one. The pore sizes were controlled by the etching duration. Finally, the AAO templates were coated with a monolayer of perfluorodecyltrichlorosilane deposited from the gas phase.[25]

PMMA with different molar masses was synthesized at 353 K by reversible addition–fragmentation chain transfer (RAFT) free radical polymerization of methyl methacrylate with 2-cyanoprop-2-yl 1-dithionaphthalate (CPDN) as a RAFT agent and 2,2′-azobisisobutyronitrile (AIBN) as an initiator in an anisole solution.[26] The molar mass and polydispersity were determined with a Waters 1515 gel permeation chromatograph equipped with a refractive-index detector and calibrated with PS standard samples. The stereoregular composition was determined with an Inova 400 MHz nuclear magnetic resonance (NMR) instrument with $CDCl_3$ as a solvent and tetramethylsilane as the internal standard. The synthesized PMMA has a molar mass by number (M_n) of 7.7, 11, 50, 140, and 360 kg mol^{-1} and a polydispersity ranging from 1.2 to 1.4. The stereoregular composition determined from ^{1}H NMR is about 35% isotactic, 4% atactic, and 61% syndiotactic (see the ESI†). Before infiltration, a thin layer (thickness ~1 μm) of polyvinyl alcohol (PVA) was deposited onto glass slides and then PMMA (~100 μm) was cast on the PVA layer. After drying the film in an ambient environment for 24 h, AAO templates were placed on top of it. To ensure good contact between the AAO template and the polymer film, the glass slide and AAO sheet were clamped and placed in a vacuum oven that was preheated to 423 K. The oven was evacuated and the sample was kept under vacuum for 5 h. Before taking the samples out, the vacuum oven was slowly cooled to room temperature. The PMMA infiltrated AAO was removed from the glass slide by dissolving PVA in water. There is no residual sample on the surface of the AAO template in this fabrication method. Before measurements, the samples were annealed at 453 K under vacuum for 24 h, and slowly cooled to room temperature (<1 K min^{-1}).

The morphology of the AAO templates and PMMA nanofibers released from the templates in a phosphoric acid/water solution was imaged with a scanning electron microscope (SEM, Hitachi S-4800) operating at 15 kV. Differential scanning calorimetry (DSC) measurements were performed with a com-

mercial differential scanning calorimeter (TA Q200) under a constant flow of nitrogen. The heating rate was 10 K min^{-1}. Dielectric relaxation spectroscopy (DRS) measurements were performed using a Novocontrol Concept-80 system at temperatures between 273 and 453 K. For bulk PMMA, the DRS measurements were carried out in the usual parallel plate geometry with electrodes of 10 mm in diameter and a sample thickness of 50 μm. For the PMMA infiltrated in the AAO templates, the 10 mm electrode was placed on the AAO surface. In all cases, the scanning was performed at a frequency of 175 Hz as a function of temperature and the complex dielectric permittivity $\varepsilon(\omega) = \varepsilon'(\omega) - i\varepsilon''(\omega)$, where ε' is the real permittivity and ε'' is the dielectric loss factor, was obtained.

Results and discussion

The morphology of AAO templates was imaged by SEM, (Fig. 1a and b), showing regular cylindrical shapes and narrow pore size distributions. The morphology and dimension of AAO nanopores were not modified by the fluoro-silanation process. We note that the regular shape and uniform size of AAO templates is one of the prerequisites for successful measurement of T_g deviations under the two-dimensional confinement. When released for observation by dissolving the AAO template, the PMMA nanofibers collapsed on the substrate but maintained their cylindrical shape (Fig. 1c and d); their length is similar to the thickness of the AAO template.

We first focus on the thermal glass transition of PMMA of a fixed molar mass (M_n = 140 kg mol^{-1}) filled in the AAO templates of various pore diameters. Fig. 2a shows the DSC heating traces of bulk and confined PMMA measured at 10 K min^{-1}. The T_g is determined from the heat flow derivative (dH/dT) in which the glass transition appears as a peak, allowing us also to observe possible broadening of the glass transition. As seen in Fig. 2b, dH/dT exhibits a relatively narrow peak centered at *ca.* 400 K for bulk PMMA ($T_{g,bulk}$). The glass transition of confined PMMA, however, appears as a broader peak, with a maximum shifting toward lower temperature for increased degrees of confinement. The broadening of the thermal glass transition indicates the dynamic heterogeneity of polymers confined in the cylindrical geometry.[27] The average T_g determined from the peak maxima is plotted in Fig. 2c as a function of the pore diameter D. Apparently, the average T_g of confined PMMA is substantially decreased in comparison to $T_{g,bulk}$ and monotonously falls with decreasing pore diameter D. The maximum T_g reduction is as large as 63.6 K in the smallest nanopores (45 nm in diameter) with respect to $T_{g,bulk}$. The relative magnitude of T_g reduction as a function of D, $\Delta T_g/T_{g,bulk} = (T_{g,bulk} - T_g)/T_{g,bulk}$, is fitted with a power law to the phenomenological model of Keddie–Jones–Cory,[28,29] which is used to describe polymer thin films supported on non-attractive substrates or freestanding films:

$$\frac{\Delta T_g}{T_{g,bulk}} = \left(\frac{A}{D}\right)^{\sigma} \quad (1)$$

where A is the characteristic length governing the glass transition and σ is the phenomenological exponent. The data fit very well with the phenomenological model. The best fit of Fig. 2b shows that A = 0.74 nm and σ = 0.44.

While DSC provides a global view of the glass transition, DRS provides dynamic structural relaxation information. Fig. 3a shows the dielectric losses ε'' measured at 175 Hz upon heating for bulk and confined PMMA. For bulk PMMA, two relaxation processes can be found from low to high temperature, corresponding to the β and α structural relaxations, respectively.[23] The α relaxation is ascribed to a long-range segmental change of the polymer backbone conformation and thus reflects the glass transition.[23] To separate the α and β relaxation processes, the dielectric loss spectra were fitted by two Gaussian functions, providing α and β relaxation maxima

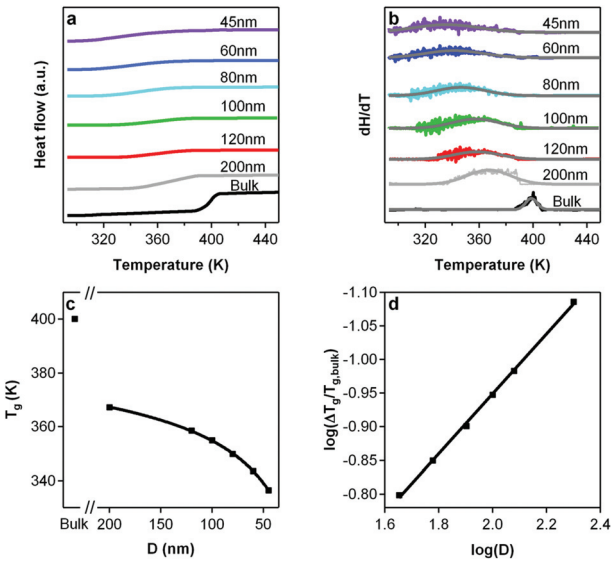

Fig. 2 Thermal glass transition of PMMA of a fixed molar mass (M_n = 140 kg mol^{-1}) confined in AAO templates of various pore diameters. (a) Normalized DSC traces of bulk PMMA and PMMA confined in AAO templates of the indicated pore diameter. (b) Derivative of the heat flow dH/dT *versus* temperature. The derivative curves are fitted by Gaussian functions to extract their maximum (grey curves). (c) T_g of bulk PMMA and confined PMMA as a function of the nanopore diameter D. (d) The relative magnitude of the depression of T_g *versus* D, and a power function fit.

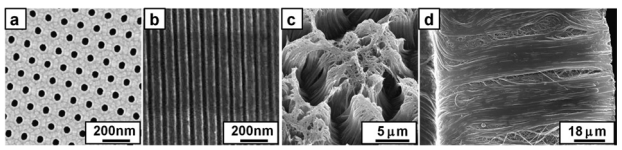

Fig. 1 The morphology of AAO templates used to bidimensionally confine polymers and the generated PMMA nanofibers with the templates. (a, b) Top and side view SEM images of an AAO template of ~80 nm pore diameter, respectively, showing the uniformity and straightness of nanopores. (c, d) Top and side view SEM images of PMMA nanofibers released from an AAO template, respectively, demonstrating the successful fabrication of PMMA nanofibers.

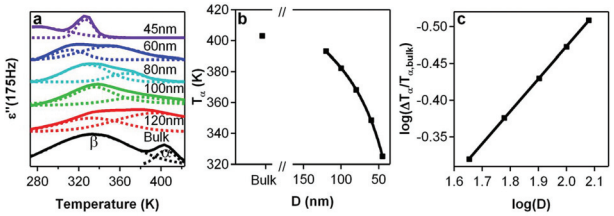

Fig. 3 Dynamic structural relaxation of PMMA of a fixed molar mass (M_n = 140 kg mol^{-1}) confined in AAO templates of various pore diameters. (a) Dielectric loss spectra of bulk PMMA and PMMA confined in AAO templates measured at 175 Hz. To guide the eye, the curves are shifted vertically. The dielectric loss curves are fitted with two independent Gaussian functions (dashed curves). (b) The dynamic glass transition temperature T_α of confined PMMA *versus* the pore diameter D. (c) The relative magnitude of the depression of T_α *versus* D, and its fit by a power function.

at *ca*. 333 and 403 K for bulk PMMA, respectively. For bulk PMMA, the DRS-determined maximum of the α relaxation peak, $T_{\alpha,bulk}$, is similar to the thermal T_g (400 K). Isochronal representations of ε'' of confined PMMA reveal a relaxation scenario completely different from the bulk sample: the low-temperature tail of the α-peaks extends well below room temperature, consistent with the thermal glass transition measured from DSC shown in Fig. 2b. The maximum of the α relaxation peak, T_α, is plotted as a function of diameter D in Fig. 3b for confined PMMA, showing that T_α monotonously shifts to lower temperatures with decreasing D, similar to DSC observations. In addition, the relative magnitude of the reduction of T_α, $\Delta T_\alpha = (T_{\alpha,bulk} - T_\alpha)/T_{\alpha,bulk}$, can also be well fitted by eqn (1) with A = 8.5 nm and σ = 0.44 (Fig. 2c). Therefore, both the macroscopic (DSC) and microscopic molecular fluctuation (DRS) measurements reveal that the T_g of PMMA confined in cylinders with non-attractive inner walls monotonously deviates from $T_{g,bulk}$. The main difference between DSC and DRS results is the characteristic length A, which differs by a factor of about 10, a fact which is not understood at the present time.

We have further investigated the glass transition of PMMA of varying M_n while fixing the nanopore diameter. Before doing so, we first checked the M_n dependence of the T_g of bulk materials, as the PMMA used here is homemade and its T_g depends on tacticity. Fig. 4a shows the heat flow traces of bulk PMMA of varying M_n measured at 10 K min^{-1} during heating.

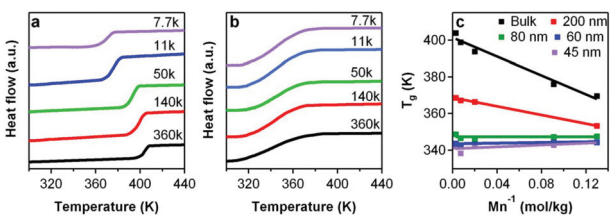

Fig. 4 The glass transition of bulk and confined PMMA of varying molar masses. (a) Normalized DSC heating traces of bulk PMMA of different molar masses (as indicated). (b) DSC traces of PMMA of various molar masses (as indicated) confined in 60 nm AAO templates. (c) The glass transition temperature T_g of bulk and confined PMMA *versus* the average molar mass by number.

As expected, T_g increases for higher M_n. Shown in Fig. 4c are the data plotted as T_g *vs.* M_n^{-1}; the data fall on a straight line, in accordance with the Fox–Flory relationship:[30]

$$\frac{1}{T_g} = \frac{1}{T_{g,\infty}} - \frac{K}{M_n} \quad (2)$$

where $T_{g,\infty}$ is the maximum glass transition temperature that can be achieved for a theoretical infinite M_n and K is an empirical parameter that is related to the extra free volume present in the sample due to the chain ends.[30] Fig. 4b shows data for PMMA of various M_n values confined in pores of a 60 nm diameter: T_g is now close to *ca.* 344 K, independent of the molar mass. This quasi-independence on the molar mass is also observed for PMMA confined in cylinders with pore diameters of 45 nm and 80 nm (Fig. 4c). For higher pore sizes (200 nm), T_g partially recovers its dependence on the molar mass, although the slope of T_g *vs.* M_n^{-1} is smaller than that for bulk PMMA (Fig. 4c).

This change of regime of the molar mass dependence provides an important clue to understand the origin for the T_g reduction of polymer nanostructures confined in non-attractive nanopores. Starting from the well-accepted notion of an equilibrium concentration of free volume in a bulk liquid, an equilibrium 'solubility' constant can be defined for the free volume. Due to entropic and enthalpic perturbations of the material close to the interface, this equilibrium constant, and therefore the concentration of free volume, is different close to the interface. Structural studies based on simulations[31] and experiments[20] have indeed revealed that spatial confinement imposed by the boundary hard walls cause a chain contraction perpendicular to the nanopore axis with fewer contact points at the interfaces, and a decreased entanglement density. In addition, packing frustration at the interface also contributes to the changing entropy at the interface.[32] Finally, van der Waals forces experienced by the liquid over a few tens of nm close to the interface, due to the surrounding membrane, are a supplementary perturbation factor. Therefore, the distribution of free volume content of PMMA confined in the nanoporous AAO templates can be schematized by a core–shell model (Fig. 5a). The shell close to the non-attractive hard walls contains a different amount of free volume, and is made of less entangled polymer chains perturbed in their entropy, enthalpy, and conformations. If the shell region is large enough to support the notion of a local T_g, this core–shell structure contributes to broaden the total glass transition and to reduce the average T_g. Furthermore, the core of the cylinders consists of polymer chains similar to those of the bulk material.

Quantitatively, taking as a hypothesis that the free volume available for segmental rearrangement is the controlling parameter, we can write the T_g at a position (r, θ, z) in the nanopore of radius R as:

$$T_g(r,\theta,z) = T_{g,0} + \frac{\partial T_g}{\partial \delta}\delta(r,\theta,z) \quad (3)$$

where T_g is the glass transition temperature in a cooperatively-rearranging region centered at a point (r, θ, z), $T_{g,0}$ is the

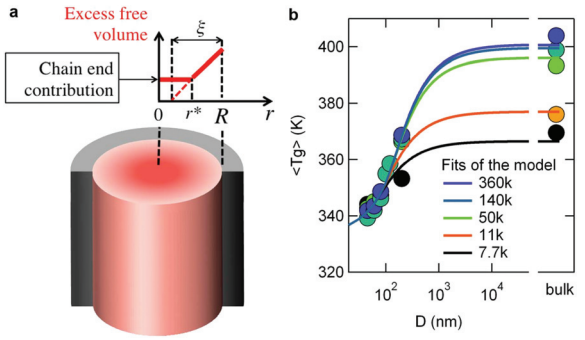

Fig. 5 The interpretation of glass transition near a hard wall in confined polymers. (a) Schematic illustration of polymers confined in bidimensional cylinders of a radius R. Spatial confinement causes conformational changes, disentanglement of polymer chains, and accumulation of excess free volume at the polymer–wall interfaces. This excess free volume is considered to decrease away from the wall according to an exponential law, until it saturates when reaching the amount of excess free volume provided by the chain ends (eqn (7)). (b) Calculated average T_g of polymers confined in cylinders based on excess free volume caused by chain ends and polymer–wall interfaces (lines, eqn (8)), compared to the experimental data (circles).

T_g of the polymer of infinite M_n in the bulk far away from interfaces, and δ is the (adimensional) volume fraction of excess free volume in a cooperatively-rearranging region at (r, θ, z):

$$\delta \triangleq \frac{v_f(r,\theta,z) - v_{f0}}{v} \tag{4}$$

where v_f is the specific free volume either at (r, θ, z) or in the reference bulk sample of the infinite molar mass (v_{f0}), and v is the specific volume of the bulk sample. The presence of the polymer–wall interface requires the creation of an equilibrium excess free volume, which we consider for simplicity to decrease away from the wall according to a linear law:

$$\delta_i(r) = \delta_0\left(1 - \frac{R-r}{\xi}\right) \quad (R - \xi \le r \le R) \tag{5}$$

where ξ is the characteristic length over which the interface is felt. This linear spatial dependence is a simple Taylor expansion limited to the first order of the unknown variation of free volume with distance from the wall; an exponentially-decreasing spatial dependence was also tested and did not lead to significantly different results.

This extra interfacial free volume needs to be created to allow the conformational perturbations to exist, unless it is already available; thanks to the free volume associated to the chain ends, which is:

$$\delta_f = \frac{n}{v}V^* = 2\frac{N_{AV}V^*}{vM_n} \triangleq f \cdot M_n{}^{-1} \tag{6}$$

with $f = 2N_{AV}V^*/v$, where n is the number of chain ends per unit mass of the sample, N_{AV} is Avogadro's number, and V^* is the free volume per chain end. Therefore, the total fraction of excess free volume compared to the bulk polymer of the infinite molar mass is (Fig. 5a):

$$\delta = \max\left(fM_n{}^{-1}, \delta_0\left(1 - \frac{R-r}{\xi}\right)\right) \tag{7}$$

This equation thus considers that the presence of the wall induces the accumulation of equilibrium excess free volume, damped away from the wall due to the existence of the characteristic length ξ; this excess free volume must be created unless it is already available; thanks to the contribution of chain ends. This is the reason for the max function appearing in eqn (7): if the chain ends provide enough excess free volume for the interfacial perturbations to exist, no supplementary extra excess free volume needs to be created. Combining eqn (3) and (7), and averaging eqn (3) over the whole volume of a nanocylinder, leads to the average glass transition temperature, $\overline{T_g}$:

$$\begin{aligned}
\overline{T_g} &= T_{g0} - \chi\delta_0\left(1 - \frac{R}{3\xi}\right), \quad \text{if } r^* \le 0 \\
\overline{T_{g0}} &= T_{g0} - \frac{\chi f}{M_n}\frac{r^{*2}}{R^2} - \chi\delta_0\left(1 - \frac{R}{\xi}\right)\left(1 - \frac{r^{*2}}{R^2}\right) \\
&\quad - \frac{2}{3}\chi\delta_0\frac{R}{\xi}\left(1 - \frac{r^{*3}}{R^3}\right), \quad \text{if } r^* \ge 0
\end{aligned} \tag{8}$$

with $\chi \triangleq -\dfrac{\partial T_g}{\partial \delta} > 0$, and $r^* = R - \xi(1 - f\delta_0{}^{-1}M_n{}^{-1})$ the radius at which the excess free volume switches from wall- to chain end-dominance (*i.e.*, $\delta_0\left(1 - \dfrac{R-r^*}{\xi}\right) = fM_n{}^{-1}$). The first expression in eqn (8) corresponds to the case for which the radius of the nanopore is so small that the free volume supplied by the chain ends is never large enough to provide the required excess. In the second case, the pore radius is large enough to have a core region, into which the excess free volume is supplied by the chain ends when $0 \le r \le r^*$.

Eqn (8) only comprises four independent parameters. It is convenient to select $T_{g,0}$, ξ, $\chi\delta_0$ and χf as fittable parameters, which can be computed by fitting eqn (8) to the experimental DSC data for all molar masses and all pore radii taken at once, including the macroscopic bulk samples. The resulting fit parameters are $T_{g,0} = 401.5 \pm 1$ K, $\xi = 60 \pm 4$ nm, $\chi\delta_0 = 69 \pm 2$ K and $\chi f = (2.7 \pm 0.2) \times 10^5$ g mol^{-1}. As seen in Fig. 5b, this simple model based on excess free volume agrees very well with our experimental observations, and is capable to capture simultaneously the effect of chain ends and polymer–wall interfaces.

The spatial range over which the excess free volume accumulates at the interface is defined by $R - r^* = \xi(1 - f\delta_0{}^{-1}M_n{}^{-1})$, and varies from 59.7 nm for the longer chains of 360 kg mol^{-1} to 29.5 nm for the shorter 7.7 kg mol^{-1} chains. For a polymer of an infinite molar mass, the interfacial spatial range is ξ = 60 nm. Hence, the interface perturbs the material over substantial distances, as experimentally confirmed before.[33,34] This range is much larger than the unperturbed radius of gyration of the chains, which varies from *ca.* 2.3 to 16 nm over the probed range of molar mass; it is however comparable to the range of van der Waals forces between extended bodies.[35]

Conclusions

Summing up, we have studied the glass transition temperature T_g of polymer nanostructures confined in nanoporous media with non-attractive inner walls. DSC and DRS measurements reveal that the T_g of PMMA substantially deviates from that of the bulk; for low pore diameters, T_g depends essentially on pore diameters, whereas it depends on the molar mass only for diameters above a few hundred nanometers. This is due to the existence of a free volume-enriched region at the interface, of *ca.* 60 nm maximal spatial range. This large range suggests that van der Waals forces must contribute significantly to the interfacial perturbation of the free volume concentration. Therefore, polymer cylinders of less than a 100 nm diameter are essentially made of interface-perturbed regions, and exhibit the same value of T_g irrespective of the molar mass. However, chains of lower molar mass supply part of the required interfacial free volume thanks to their chain end contribution, resulting in smaller depressions of T_g compared to polymers of higher molar mass. The simple model we propose is able to provide a consistent interpretation of the glass transition of polymer nanostructures in confinement, which should allow us to predict the variation of the glass transition temperature with a molar mass and the degree of confinement for a variety of confining geometries.

Acknowledgements

This work was supported by the National Basic Research Program of China (no. 2012CB821500), the National Natural Science Foundation of China (no. 51473112), a Project for Jiangsu Scientific and Technological Innovation Team (2013), a Project Funded by the Priority Academic Program Development of Jiangsu Higher Education Institutions (PAPD), and the Belgian Federal Science Policy (IAP program P7/05).

Notes and references

1 Z. Hu, M. Tian, B. Nysten and A. M. Jonas, *Nat. Mater.*, 2009, **8**, 62.
2 L. Nyholm, G. Nyström, A. Mihranyan and M. Strømme, Toward flexible polymer and paper-based energy storage devices, *Adv. Mater.*, 2011, **23**, 3751–3769.
3 S. Ghosh, N. A. Kouamé, L. Ramos, S. Remita, A. Dazzi, A. Deniset-Besseau, P. Beaunier, F. Goubard, P.-H. Aubert and H. Remita, *Nat. Mater.*, 2015, **14**, 505.
4 D. Bratton, D. Yang, J. Y. Dai and C. K. Ober, *Polym. Adv. Technol.*, 2006, **17**, 94.
5 S. Y. Chou, P. R. Krauss and P. J. Renstrom, *Science*, 1996, **272**, 85.
6 Y. N. Xia and G. M. Whitesides, *Angew. Chem., Int. Ed.*, 1998, **37**, 550.
7 J. I. Lee, S. H. Cho, S. M. Park, J. K. Kim, J. K. Kim, J. W. Yu, Y. C. Kim and T. P. Russell, *Nano Lett.*, 2008, **8**, 2315.
8 R. Cai, H. G. Kassa, R. Haouari, A. Marrani, Y. H. Geerts, C. Ruzié, A. J. J. M. van Breemen, G. H. Gelinck, B. Nysten, Z. Hu and A. M. Jonas, *Nanoscale*, 2016, **8**, 5968.
9 T. P. Russell, *Science*, 2013, **341**, 1351.
10 E. Woo, J. Huh, Y. G. Jeong and K. Shin, *Phys. Rev. Lett.*, 2007, **98**, 136103.
11 Z. Hu and A. M. Jonas, *Soft Matter*, 2010, **6**, 21.
12 J. L. Lutkenhaus, K. McEnnis, A. Serghei and T. P. Russell, *Macromolecules*, 2010, **43**, 3844.
13 H. G. Chae and S. Kumar, *Science*, 2008, **319**, 908.
14 Y. Wu, Q. Gu, G. Ding, F. Tong, Z. Hu and A. M. Jonas, *ACS Macro Lett.*, 2013, **2**, 535.
15 V. Singh, T. L. Bougher, A. Weathers, Y. Cai, K. Bi, M. T. Pettes, S. A. McMenamin, W. Lv, D. P. Resler, T. R. Gattuso, D. H. Altman, K. H. Sandhage, L. Shi, A. Henry and B. A. Cola, *Nat. Nanotechnol.*, 2014, **9**, 384.
16 Z. Hu, B. Muls, L. Gence, D. A. Serban, J. Hofkens, S. Melinte, B. Nysten, S. Demonstier-Champagne and A. M. Jonas, *Nano Lett.*, 2007, **7**, 3639.
17 M. K. Mundra, S. K. Donthu, V. P. Dravid and J. M. Torkelson, *Nano Lett.*, 2007, **7**, 713.
18 Y. Ding, H. W. Ro, T. A. Germer, J. F. Douglas, B. C. Okerberg, A. Karim and C. L. Soles, *ACS Nano*, 2007, **1**, 84.
19 Y. Ding, H. W. Ro, J. F. Douglas, R. L. Jones, D. R. Hine, A. Karim and C. L. Soles, *Adv. Mater.*, 2007, **19**, 1377.
20 K. Shin, S. Obukhov, J.-T. Chen, J. Hun, Y. Hwang, S. Mok, P. Dobriyal, P. Thiyagarajan and T. P. Russell, *Nat. Mater.*, 2007, **6**, 961.
21 H. Duran, A. Gitsas, G. Fluodas, M. Nondeshki, M. Steinhart and W. Knoll, *Macromolecules*, 2009, **42**, 2881.
22 L. Li, D. Zhou, D. Huang and G. Xue, *Macromolecules*, 2014, **47**, 297.
23 Y. Sha, L. Li, X. Wang, Y. Wan, J. Yu, G. Xue and D. Zhou, *Macromolecules*, 2014, **47**, 8722.
24 I. Blaszczyk-Lezak, M. Hernández and C. Mijangos, *Macromolecules*, 2013, **46**, 4995.
25 A. Pallandre, K. Glinel, A. M. Jonas and B. Nysten, *Nano Lett.*, 2004, **4**, 365.
26 Z. Zhang, W. Wang, H. Xia, J. Zhu, W. Zhang and X. Zhu, *Macromolecules*, 2009, **42**, 7360.
27 G. Adam and J. H. Gibbs, *J. Chem. Phys.*, 1965, **43**, 139.
28 J. L. Keddie, R. A. L. Jones and R. A. Cory, *Europhys. Lett.*, 1994, **27**, 59.
29 J. L. Keddie, R. A. L. Jones and R. A. Cory, *Faraday Discuss.*, 1994, **98**, 219.
30 T. G. Fox Jr. and P. J. Flory, *J. Appl. Phys.*, 1950, **21**, 581–591.
31 D. M. Sussman, W.-S. Tung, K. I. Winey, K. S. Schweizer and R. A. Riggleman, *Macromolecules*, 2014, **47**, 6462.
32 S. Napolitano, C. Rotella and M. Wübbenhorst, *ACS Macro Lett.*, 2012, **1**, 1189.
33 R. D. Priestley, C. J. Ellison, L. J. Broadbelt and J. M. Torkelson, *Science*, 2005, **309**, 456.
34 C. J. Ellison and J. M. Torkelson, *Nat. Mater.*, 2003, **2**, 695.
35 J. Israelachvili, *Intermolecular & Surface Forces*, Acamdemic Press Limited, 2nd edn, 1991, ch. 11, pp. 176–212.